*J. Fluid Mech.* (2004), *vol.* 521, *pp.* 273–294.  
DOI: 10.1017/S0022112004001776 Printed in the United Kingdom

# Optimal large-eddy simulation results for isotropic turbulence

By JACOB A. LANGFORD† AND ROBERT D. MOSER

Department of Theoretical and Applied Mechanics, University of Illinois
104 S Wright Street, Urbana, IL 61801-2983, USA

(Received 30 March 2004 and in revised form 20 August 2004)

A new class of large-eddy simulation (LES) models (optimal LES) was previously introduced by the authors. These models are based on multi-point statistical information, which here is provided by direct numerical simulation (DNS). In this paper, the performance of these models in LES of forced isotropic turbulence is investigated. It is found that both linear and quadratic optimal models yield good simulation results, with an excellent match between the LES and filtered DNS for spectra, and low-order structure functions.

Optimal models were then used as a vehicle to investigate the effects of filter shape and the locality of model dependence on LES performance. Results indicate that a Fourier cutoff filter yields more accurate simulations than graded cutoff filters, leaving no motivation to use graded filters in spectral simulations. It was also found that optimal models formulated to depend on local information performed nearly as well as global models. This is important because in practical LES simulations in which spectral methods are not applicable, global model dependence would be prohibitively expensive.

## 1. Introduction

Large-eddy simulation of turbulence (LES) is a simulation technique whereby only the largest scales are simulated and a model is used to account for the missing small-scales (see Rogallo & Moin 1984). Such a simulation is motivated by the recognition that the large scales of turbulence often dominate heat transfer, mixing and other quantities of engineering interest, whereas the small scales of turbulence are important in these cases only because they affect the large scales. There has been optimism that LES can be used as a robust predictive tool, partly because the small scales of turbulence are believed to be more isotropic and more universal than the large scales, and partly because LES has already been successful in many flows. For reviews of LES see Rogallo & Moin (1984); Lesieur & Métais (1996); Meneveau & Katz (2000).

To formulate an LES, we must first define the large scales to be simulated, which is accomplished by way of a spatial low-pass filter. The filtered velocity $\tilde{u}_i(\boldsymbol{x})$ is generally defined:

$$\tilde{u}_i(\boldsymbol{x}) = \int g(\boldsymbol{x}, \boldsymbol{x}')u_i(\boldsymbol{x}')\,\mathrm{d}\boldsymbol{x}', \tag{1.1}$$

† Present address: Sony Computer Entertainment of America, 10075 Barnes Canyon Rd, San Diego, CA 92121, USA.

where $g$ is the filter kernel. When $g$ depends only on $\boldsymbol{x}' - \boldsymbol{x}$ it is said to be homogeneous and in this case, the filter operator commutes with spatial differentiation. Applying a homogeneous filter to the Navier–Stokes equations yields

$$\frac{\partial \widetilde{u}_i}{\partial t} = -\frac{\partial \widetilde{\widetilde{u}_i \widetilde{u}_j}}{\partial x_j} - \frac{\partial \widetilde{p}}{\partial x_i} + \frac{1}{Re}\frac{\partial^2 \widetilde{u}_i}{\partial x_j \partial x_j} + M_i, \tag{1.2}$$

where $M_i = \partial \tau_{ij}/\partial x_j$ is the subgrid model term, and $\tau_{ij} = \widetilde{\widetilde{u}_i \widetilde{u}_j} - \widetilde{u_i u_j}$ is the subgrid stress. It remains to determine a model for the subgrid force $M_i$, or more commonly the subgrid stress $\tau_{ij}$.

A large number of subgrid stress models have been proposed in the literature (e.g. Smagorinsky 1963; Bardina, Ferziger & Reynolds 1980; Métais & Lesieur 1992; Liu, Meneveau & Katz 1994). Perhaps the most common is the dynamic Smagorinsky model first proposed by Germano *et al.* (1991), and subsequently refined by several authors (Lilly 1992; Ghosal *et al.* 1995; Meneveau, Lund & Cabot 1996). While the dynamic Smagorinsky model as well as others have been used successfully to simulate a variety of flows, there continue to be unresolved issues regarding LES formulations and shortcomings in LES models in important flows (e.g. wall-bounded flows).

To address some of these shortcomings, Langford & Moser (1999) proposed a class of models (optimal LES models) based on formal optimization of the subgrid model term, similar to the previous proposal by Adrian (1977, 1990). Such models were shown to approximate formally the ideal subgrid model, a well-defined, though impractical to compute, LES model that guarantees correct large-scale statistics while minimizing the mean-square difference between the exact and modelled subgrid force term (Langford & Moser 1999; Pope 2000). In this paper, the performance of optimal LES models in forced isotropic turbulence is evaluated. These models are formulated using statistical data from a direct numerical simulation (DNS) of forced isotropic turbulence (Langford & Moser 1999). The models are also used as a platform to investigate two other important issues in LES formulation: the effect of filter definition on the accuracy of LES models and simulations, and the importance of non-local information in the formulation of LES models. In the following subsections, the optimal LES approach is briefly reviewed, and the context of the filter and non-locality issues are described.

### 1.1. *Filtering, discretization and LES*

Filtering plays a pivotal role in LES, in that it defines precisely the large scales to be simulated. There is, however, an interaction between filtering and discretization which is of critical importance to the optimal LES formulation. There are, in fact, two distinct approaches to filtering and discretization, which are described here.

(*a*) *Continuous filtering*. In continuous filtering, a filter (e.g. a Gaussian or top-hat) as defined in (1.1) is used, resulting in the filtered Navier–Stokes equations, (1.2). A model for subfilter stress is then introduced and the resulting PDE is discretized in space and solved numerically. This is the more common formulation.

(*b*) *Discrete filtering*. In discrete filtering, a filter is defined as a (linear) mapping from the infinite dimensional space in which Navier–Stokes solutions evolve to a finite dimensional space, which can be represented on a computer without further spatial discretization. In essence, discretization or truncation has been included in the filter definition. Examples of such filters include the Fourier cutoff filter (in a finite periodic domain), and finite volume filters (Zandonade, Langford & Moser 2004). (Note that the filter as defined in (1.1) can be generalized to include such a discretization, if $g$ can be a distribution.) In this case, the modelling is done in the resulting dynamical system,

rather than a partial differential equation as with continuous filters. This approach is used for cutoff filtered LES, MILES (Boris *et al.* 1992) and in optimal LES.

There are advantages and disadvantages to each of these approaches. An advantage of the continuous approach is that we can use standard numerical techniques and control numerical errors in the usual way through grid refinement. In short, the numerical solution should converge to the solution of the LES PDEs. The disadvantage is that this is expensive, it requires resolution that is much finer than the filter width, so that it is rarely done in practice. In the discrete filtering approach, we cannot even consider convergence of the spatial numerical discretization, because there is none. There are only modelling errors. This is an advantage because it can lead to cheaper LES, and a disadvantage because we cannot use the usual numerical convergence as a quality control tool.

If we ask what is the best possible LES model for a particular problem, as we do in optimal LES, then the discrete filtering approach is compelling. The reason is that in most cases the continuous filter is invertible or nearly so. For example, a Gaussian filter is formally invertible (the Fourier transform of the kernel is real and positive). A top-hat filter is nearly invertible in that the kernel Fourier transform is real and non-zero for all but a countable set of wavenumbers. In either case, the filtered field contains much information about the small-scale turbulence. The best possible model would use all of this available information. In particular, for an invertible filter, the best model would exactly reproduce the subgrid term. This would be equivalent to a DNS with different dependent variables, and the numerical resolution requirements would be the same as for a DNS. When we discretize the equations using resolution appropriate for LES, the small-scale information in the filtered field is discarded. Thus, in this approach, it is primarily the discretization that limits the small-scale information that is available, and therefore limits the possible accuracy of the LES model. Indeed, models that are based on the reconstruction of the small scales (approximate inversion of the filter) require additional model or regularization terms owing to the discretization (e.g. Stolz, Adams & Kleiser 2001; Domaradzki & Adams 2002). For this reason, we are led to include the discretization in the definition of the filter, so it can be accounted for in the modelling.

Similar observations have been made by a number of authors (Zhou, Hossain & Vahala 1989; Langford & Moser 1999; Domaradzki & Loh 1999; Winckelmans *et al.* 2001; Carati, Winckelmans & Jeanmart 2001), which have led some to distinguish between the (invertible) 'filter' and the (non-invertible) numerical 'truncation', and to account for both in the modelling process (Carati *et al.* 2001; Winckelmans *et al.* 2001). For optimal LES, this distinction is not necessary. It will suffice to consider the filter to be a mapping to the discrete space in which the LES simulation will be performed as described for the discrete filtering approach. There are then many turbulent fields (formally infinite) that map to the same LES state, and the key to the optimal LES formulation is to consider averages over these fields.

### 1.2. *Ideal and optimal LES*

*Ideal large-eddy simulation* is so called because it is the deterministic LES that yields both the most accurate statistics and the most accurate large-scale dynamics, as described below. The essential features of ideal LES are reviewed here, but for a more thorough introduction see Langford & Moser (1999).

The evolution equation for ideal LES is

$$\frac{\partial w_i}{\partial t}(\boldsymbol{x}) = \left\langle \widetilde{\frac{\partial u_i}{\partial t}}(\boldsymbol{x}) \middle| \widetilde{\boldsymbol{u}}(\boldsymbol{x}') = \boldsymbol{w}(\boldsymbol{x}') \text{ for all } \boldsymbol{x}' \right\rangle. \tag{1.3}$$

where $\tilde{\cdot}$ is the filter operator, $w_i$ is the LES velocity and $u_i$ is the real turbulent velocity. Here and throughout, $\langle\cdot\rangle$ represents the expected value, while $\langle\cdot|\cdot\rangle$ is the conditional expectation. The ideal evolution (1.3) is founded on the observation that in the absence of information about the small scales, there is a distribution of possible large-scale evolutions associated with any given filtered field. The ideal LES evolution expressed in (1.3) is simply the average over this distribution. A simulation with such an evolution is guaranteed to match any one-time statistical quantity of the filtered turbulence (Langford & Moser 1999; Pope 2000). Further, the mean-square difference between $\partial \boldsymbol{w}/\partial t$ and $\widetilde{\partial \boldsymbol{u}/\partial t}$ is minimized.

The LES equations are typically expressed as Navier–Stokes terms operating on the filtered velocity field $w_i(\boldsymbol{x})$ plus a model term $m_i(\boldsymbol{x})$ as in (1.2). Ideal LES is achieved when the model is chosen as a conditional average of the true subgrid force $M_i(\boldsymbol{x})$:

$$m_i(\boldsymbol{x}) = \langle M_i(\boldsymbol{x}) | \tilde{\boldsymbol{u}}(\boldsymbol{x}') = \boldsymbol{w}(\boldsymbol{x}') \text{ for all } \boldsymbol{x}' \rangle. \tag{1.4}$$

Note that the condition in (1.3) and (1.4) is a match of large-scale velocity over the entire domain; hence, the information required to represent the ideal evolution equations, or equivalently an ideal subgrid model, is prohibitive.

An *optimal LES formulation* is a formal approximation to ideal LES, using stochastic estimation (Adrian *et al.* 1989). The quadratic estimate

$$m_i(\boldsymbol{x}) = A_i(\boldsymbol{x}) + \int B_{ij}(\boldsymbol{x}, \boldsymbol{x}') w_j(\boldsymbol{x}') \, \mathrm{d}\boldsymbol{x}' + \int C_{ijk}(\boldsymbol{x}, \boldsymbol{x}') w_j(\boldsymbol{x}') w_k(\boldsymbol{x}') \, \mathrm{d}\boldsymbol{x}' \tag{1.5}$$

has been previously studied because this form subsumes the terms in the incompressible Navier–Stokes equations, so that modelling the subgrid force $M_i$ and the time derivative $\partial w_i/\partial t$ are equivalent (this equivalence is always true for the ideal formulation, but need not be for optimal forms). However, any set of terms can be introduced, and provided that appropriate flow statistics are available (two-point second-, third- and fourth-order correlations for the quadratic estimate shown), the optimal estimation kernels $A_i(\boldsymbol{x})$, $B_{ij}(\boldsymbol{x}, \boldsymbol{x}')$ etc. can be found.

The estimation kernels are determined by minimizing the mean-square difference between $m_i$ and $M_i$ (Adrian *et al.* 1989), yielding the following system of integral equations:

$$\langle M_i(\boldsymbol{x}) \rangle = A_i(\boldsymbol{x}) + \int B_{ij}(\boldsymbol{x}, \boldsymbol{x}') \langle \tilde{u}_j(\boldsymbol{x}') \rangle \, \mathrm{d}\boldsymbol{x}' + \int C_{ijk}(\boldsymbol{x}, \boldsymbol{x}') \langle \tilde{u}_j(\boldsymbol{x}') \tilde{u}_k(\boldsymbol{x}') \rangle \, \mathrm{d}\boldsymbol{x}', \tag{1.6}$$

$$\langle \tilde{u}_l(\boldsymbol{x}'') M_i(\boldsymbol{x}) \rangle = A_i(\boldsymbol{x}) \langle \tilde{u}_l(\boldsymbol{x}'') \rangle + \int B_{ij}(\boldsymbol{x}, \boldsymbol{x}') \langle \tilde{u}_l(\boldsymbol{x}'') \tilde{u}_j(\boldsymbol{x}') \rangle \, \mathrm{d}\boldsymbol{x}' + \int C_{ijk}(\boldsymbol{x}, \boldsymbol{x}') \langle \tilde{u}_j(\boldsymbol{x}') \tilde{u}_k(\boldsymbol{x}') \rangle \, \mathrm{d}\boldsymbol{x}', \tag{1.7}$$

$$\langle \tilde{u}_l(\boldsymbol{x}'') \tilde{u}_m(\boldsymbol{x}'') M_i(\boldsymbol{x}) \rangle = A_i(\boldsymbol{x}) \langle \tilde{u}_l(\boldsymbol{x}'') \tilde{u}_m(\boldsymbol{x}'') \rangle + \int B_{ij}(\boldsymbol{x}, \boldsymbol{x}') \langle \tilde{u}_l(\boldsymbol{x}'') \tilde{u}_m(\boldsymbol{x}'') \tilde{u}_j(\boldsymbol{x}') \rangle \, \mathrm{d}\boldsymbol{x}' + \int C_{ijk}(\boldsymbol{x}, \boldsymbol{x}') \langle \tilde{u}_l(\boldsymbol{x}'') \tilde{u}_m(\boldsymbol{x}'') \tilde{u}_j(\boldsymbol{x}') \tilde{u}_k(\boldsymbol{x}') \rangle \, \mathrm{d}\boldsymbol{x}'. \tag{1.8}$$

To determine the estimation kernels, the two-point correlations of the filtered velocities are required. In Langford & Moser (1999), and in this paper, these statistical correlations are obtained from direct numerical simulations (DNS) of isotropic turbulence at $Re_\lambda = 164$.

To assess the quality of a particular estimate, the estimation difference $d_i(\boldsymbol{x}) = M_i(\boldsymbol{x}) - m_i(\boldsymbol{x})$ is measured in a mean-square sense. We refer to this as estimation

difference, to distinguish it from the error $e_i(\boldsymbol{x}) = \langle M_i(\boldsymbol{x}) | \tilde{\boldsymbol{u}} = \boldsymbol{w} \rangle - m_i(\boldsymbol{x})$, which is the difference between the ideal model and the model under consideration. Error is not an appropriate term for $d_i$, since it cannot be made arbitrarily small, though $e_i$ can. Unfortunately, since we do not know the ideal model, we cannot determine the error $e_i$. However, if the estimation difference is larger in one case than another, it follows that the error is also larger.

It was shown in Langford & Moser (1999) that for forced isotropic turbulence, the magnitude of the estimation difference is nearly as large as the magnitude of the true subgrid force, even with a model containing 46 terms chosen to subsume many common subgrid models. This result suggests that the mean-square estimation difference of the ideal model (the smallest possible) may be similarly large. If so, then most of the subgrid force cannot be expressed as a deterministic function of the filtered field, and is in this sense stochastic. This implies that there are limitations on the small-scale effects that can be represented using deterministic models. For example, in isotropic turbulence, the often cited energy backscatter, in which locally (in space and time) energy is transferred from small scales to large scales, appears to be a stochastic effect, not representable by deterministic models (Langford & Moser 1999). In this context, we might question the advisability of relying on deterministic models, and consider adding a stochastic (random) component to the model. However, the properties of the (deterministic) ideal model (Langford & Moser 1999) indicate that this is not necessary for the prediction of large-scale single-time statistics.

In the previous optimal LES work, it was also found that the dominant term of the estimate was the linear, purely dissipative, term. For isotropic turbulence, this is equivalent to a wavenumber-dependent eddy viscosity. In Fourier space,

$$\hat{m}_i(\boldsymbol{k}) = -k^2 \hat{\nu}_T(k) \hat{w}_i(\boldsymbol{k}), \tag{1.9}$$

where $\hat{\nu}_T$ is the eddy viscosity, $\boldsymbol{k}$ is the wavevector, and $k$ is the magnitude of $\boldsymbol{k}$. The optimal eddy-viscosity $\hat{\nu}_T$ has the well-known plateau–cusp behaviour predicted by Kraichnan (1976).

It was shown in Langford & Moser (1999) that the simple linear estimate of (1.9) is capable of exactly capturing the detailed wavenumber-by-wavenumber energy transfer (on average) between the resolved and subgrid velocity scales as well as all the subgrid terms in the evolution equation for the filtered two-point velocity correlation, when measured in an *a priori* test.

As an example, the joint probability density of $\hat{M}_{\parallel}(\boldsymbol{k})$ and $\hat{\tilde{u}}(\boldsymbol{k})$ and the conditional average $\langle \hat{M}_{\parallel}(\boldsymbol{k}) | \hat{\tilde{u}}(\boldsymbol{k}) \rangle$ are shown in figure 1 for $15 < k < 16$ in isotropic turbulence with a Fourier cutoff filter ($k_c = 16$). Here, $\hat{M}_{\parallel}$ is the component of the Fourier transformed subgrid force $M_i$ parallel to $\hat{\tilde{\boldsymbol{u}}}$, and $\hat{\tilde{u}}(\boldsymbol{k})$ is the magnitude of the filtered velocity Fourier transform. The wavenumber shell $15 < k < 16$ is selected for this example because the subgrid force magnitude is largest in this range. The probability density contours and conditional average confirm that the relationship between subgrid force magnitude and large-scale velocity magnitude is approximately linear, though the variance is large. It is thus expected that the optimal linear and higher-order models proposed by Langford & Moser (1999) will produce accurate large-eddy simulation. Results of several such simulations are examined in § 2 to test this supposition.

### 1.3. *Filter choices*

In homogeneous turbulence, the most natural choice for an LES filter is the Fourier cutoff filter, in which the Fourier representation of the velocity is truncated at some cutoff wavenumber $k_c$. However, a variety of other choices are possible.

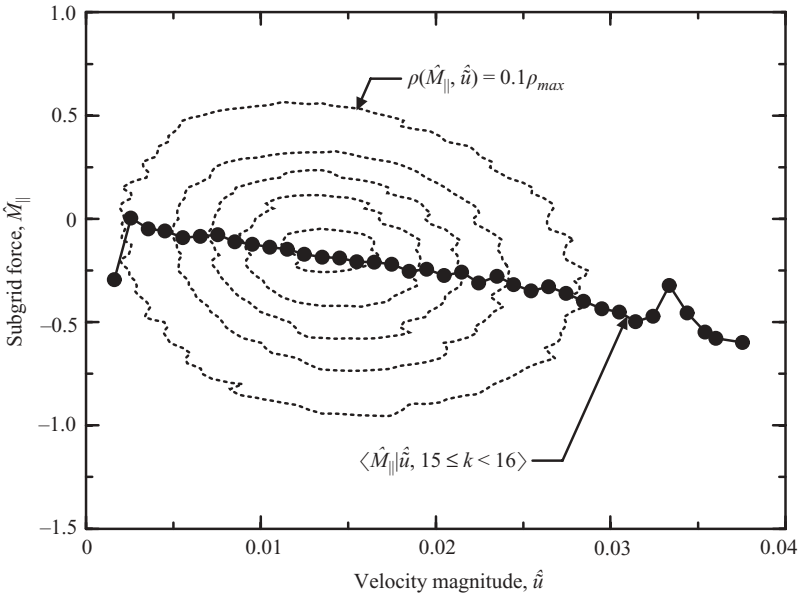


FIGURE 1. Contours of probability density $\rho(\hat{M}_{\|}, \hat{u})$, and the conditional average of $\hat{M}_{\|}$ given $\hat{u}$, where $\hat{u} = \sqrt{\hat{u}_i \hat{u}_i^*}$, the spectral velocity magnitude, and $\hat{M}_{\|} = \hat{M}_i \hat{u}_i / \hat{u}$, the component of subgrid force parallel to $\hat{\boldsymbol{u}}$. Data are shown for $15 < k < 16$, and the Fourier filter cutoff is $k_c = 16$. This figure demonstrate the applicability of (1.9) to raw data.

It was observed by Clark, Ferziger & Reynolds (1979) that the subgrid stress associated with a sharp Fourier-cutoff filter has different properties to the stress associated with a Gaussian filter. For example, the characteristic plateau–cusp $k$-dependent eddy-viscosity behaviour (Kraichnan 1976; Domaradzki *et al.* 1987; Lesieur & Rogallo 1989), is unique to the cutoff filter. Also, there has been criticism that the sharp Fourier-cutoff filter is subject to Gibbs phenomenon, which may mask the deterministic nature of the subgrid term (see Meneveau & Katz 2000; Leslie & Quarini 1979). Further, it was pointed out by Vreman, Geurts & Kuerten (1994) that Fourier curoff filters do not produce subgrid stresses $\tau_{ij}$ that are positive semi-definite as the Reynolds stress tensor is. While the positivity property is certainly not required, it may be convenient in modelling since it results in realizability constraints on the models. In the current deterministic discrete LES context, however, it is not the positivity of $\tau_{ij}$ that is relevant, but rather its conditional average $\langle \tau_{ij} | \tilde{\boldsymbol{u}} \rangle$. It is not currently known whether the conditional averaged stress has the positivity property with Fourier cutoff filters.

Two commonly proposed alternatives to the sharp cutoff filter are the Gaussian filter and the top-hat filter. However, as discussed in § 1.1, these filters are invertible or nearly so. For optimal LES, if such filters are used, the discretization must also be included. Here, the Gaussian or top-hat filter is coupled with a Fourier cutoff filter. This is what occurs implicitly when a Fourier spectral method is used.

The intrinsic limits of large-eddy simulation, which are realized by the ideal model, arise from the relationship between the LES phase space and the phase space of the real system. The filters in common use for LES are linear. As was shown in Langford & Moser (1999), they can in general be decomposed into a linear projection followed by an invertible linear transformation. For ideal LES, it is the projection that

establishes what properties an LES will have; the invertible part of the transformation is nothing more than a change of dependent variables.

While the use of a graded filter has no impact on ideal LES, if it is invertible, when optimal LES formulations or any of the common practical 'non-ideal' models are used, graded filters can have an impact. The reason is that the graded filter affects the computation of the nonlinear and model terms. Because the functional form of the optimal or other model is constrained, it is not generally possible for the effect of the graded filter on the nonlinear terms to be exactly cancelled by the effect on the model. In § 3, we investigate this impact, and in particular whether the change of variables introduced by an invertible transformation is useful in improving LES models.

### 1.4. *Model non-locality*

The optimal LES formulations studied in Langford & Moser (1999) and §§ 2–3 are based on convolutions of estimation kernels with event data from the entire field. That is, the model evaluated at any point is dependent on the LES velocity everywhere in the spatial domain. In practical simulations, we typically do not use spectral representations, like those used here, but rather finite-element, finite-volume, or finite-difference representations. In these non-spectral representations, the use of global event data leads to full matrices that are expensive to solve. To reduce this cost, we would like to restrict the estimation to nearby event data. Furthermore, the global nature of the optimal models distinguishes them from most currently used LES models, though some models such as the dynamic procedure and scale similarity models can be interpreted as using non-local information.

The question arises then as to how important non-local dependence is to subgrid mode performance. This is investigated in § 4 by restricting the dependence of optimal models to velocities at points close to the evaluation point of the model.

## 2. Optimal LES results

To evaluate the performance of the optimal models proposed by Langford & Moser (1999), they were implemented in an LES code for forced isotropic turbulence using Fourier spectral methods and a Fourier cutoff filter (the filter for which the models were constructed). Simulations were then performed for the same case as the DNS from which the correlations required in the optimal estimates were obtained, and the results compared to those for the filtered DNS. The results of this comparison are presented here.

Owing to homogeneity and isotropy, the linear and quadratic optimal estimation models as given in (1.5) can be written as corrections to the viscous and advection terms of the Navier–Stokes equations. So, when they are implemented in the simulation, the equations to be solved, in Fourier-space, are

$$\frac{\partial \hat{w}_i}{\partial t} = (\hat{L}(k) - \nu k^2)\hat{w}_i + (\hat{Q}(k) - 1)\mathscr{P}_{ilj}(\widehat{w_l w_j}) + \tilde{f}(k), \tag{2.1}$$

where $\tilde{f}(k)$ is the filtered large-scale forcing used in the direct numerical simulation, $\hat{L}(k)$ and $\hat{Q}(k)$ are the Fourier transformed optimal estimation kernels, which can be shown to be scalars due to isotropy, and

$$\mathscr{P}_{ilj}(\boldsymbol{k}) = \mathrm{i}k_j(\delta_{il} - k_i k_l/k^2) \tag{2.2}$$

is just $\mathrm{i}k_j$ times the divergence-free projection operator. The estimation kernels are determined by solving the following system of algebraic equations at each

| | DNS | LES |
|---|---|---|
| $Re_\lambda$ | 164 | 164 |
| Box size $L$ | $2\pi$ | $2\pi$ |
| Grid size | $256^3$ | $32^3$ |
| Cutoff wavenumber $k_c$ | – | 16 |
| Forced wavenumbers | $k \leqslant 3$ | $k \leqslant 3$ |
| $k_{max}\eta$ | 1 | 0.13 |

TABLE 1. Simulation parameters for the LES and for the DNS used to generate statistics for formulating the optimal models and to compare with LES results. All simulations were performed using de-aliased spectral methods in a cubical box with periodic boundary conditions. $k_{max}$ is the maximum wavenumber in the simulation, $\eta$ is the Kolmogorov length scale. All LES use a Fourier cutoff filter, those in § 3 also use a graded filter.

wavenumber, which is just the Fourier transformed isotropic version of (1.6–1.8):

$$\langle \hat{\tilde{u}}_i(\boldsymbol{k})\hat{M}_i(\boldsymbol{k})\rangle = \hat{L}(\boldsymbol{k})\langle \hat{\tilde{u}}_i(\boldsymbol{k})\hat{\tilde{u}}_i(\boldsymbol{k})\rangle + \hat{Q}(\boldsymbol{k})\langle \hat{\tilde{u}}_i(\boldsymbol{k})\mathscr{P}_{ilj}(\widehat{\tilde{u}_l\tilde{u}_j})(\boldsymbol{k})\rangle, \tag{2.3}$$

$$\begin{aligned}\langle \mathscr{P}_{ilj}(\widehat{\tilde{u}_l\tilde{u}_j})(\boldsymbol{k})\hat{M}_i(\boldsymbol{k})\rangle &= \hat{L}(\boldsymbol{k})\langle \mathscr{P}_{ilj}(\widehat{\tilde{u}_l\tilde{u}_j})(\boldsymbol{k})\hat{\tilde{u}}_i(\boldsymbol{k})\rangle \\ &\quad + \hat{Q}(\boldsymbol{k})\langle \mathscr{P}_{ilj}(\widehat{\tilde{u}_l\tilde{u}_j})(\boldsymbol{k})\mathscr{P}_{imn}(\widehat{\tilde{u}_m\tilde{u}_n})(\boldsymbol{k})\rangle.\end{aligned} \tag{2.4}$$

In the simulation code that implements these models, the nonlinear terms are fully dealiased and are time-advanced with a second-order Runge–Kutta scheme; linear terms are time-advanced with an integrating factor. This is the time-advancement treatment used in the DNS. Also implemented is the Smagorinsky model, and dynamic Smagorinsky model.

Parameters used for the simulations are shown in table 1, along with those for the DNS from which the optimal models were derived, and to which the comparisons are made. The filter cutoff, $k_c = 16$, is the coarsest filter studied by Langford & Moser (1999) and was chosen for this study because it is in the approximate inertial range of the DNS. Simulations were performed for the optimal linear model ($L^{16}$), the optimal quadratic model ($Q^{16}$), and several cases of the Smagorinsky model. One Smagorinsky simulation was conducted with $C_s = 0.819$, an optimal value that *a priori* minimizes r.m.s. error between the model and the subgrid force. A Smagorinsky model with the usual value of the constant $C_s = 0.17$ was also used, along with the dynamic Smagorinsky.

The three-dimensional energy spectra $E(k)$ for the various LES models are shown in figure 2. The optimal Smagorinsky model is grossly overly dissipative, thus illustrating that the *a priori* error minimization problem is not guaranteed to produce the best *a posteriori* results for arbitrary estimates; it is only guaranteed to produce the best *a posteriori* results for the unconstrained optimization leading to the conditional average in (1.4). With a Smagorinsky constant of $C_s = 0.17$, the results are much better, though a discrepency is still apparant, as is the case for the dynamic Smagorinsky model. The optimal linear and quadratic models, however, do an excellent job of reproducing the correct energy spectrum. There is a slight discrepancy between the DNS and optimal LES energy spectra in the middle part of the spectrum ($k \approx 4$), but it is possible that this discrepancy is due to the limited statistical sample of the DNS. Also, it is apparent that there is a slight upward hook at the tail of $E(k)$ for $L^{16}$, and that this hook is corrected somewhat in $Q^{16}$. This hook is an indication of a slightly under-dissipative model near the cutoff. However, both the $L^{16}$ and $Q^{16}$ models are constructed to exactly reproduce the $k$-dependent energy transfer to

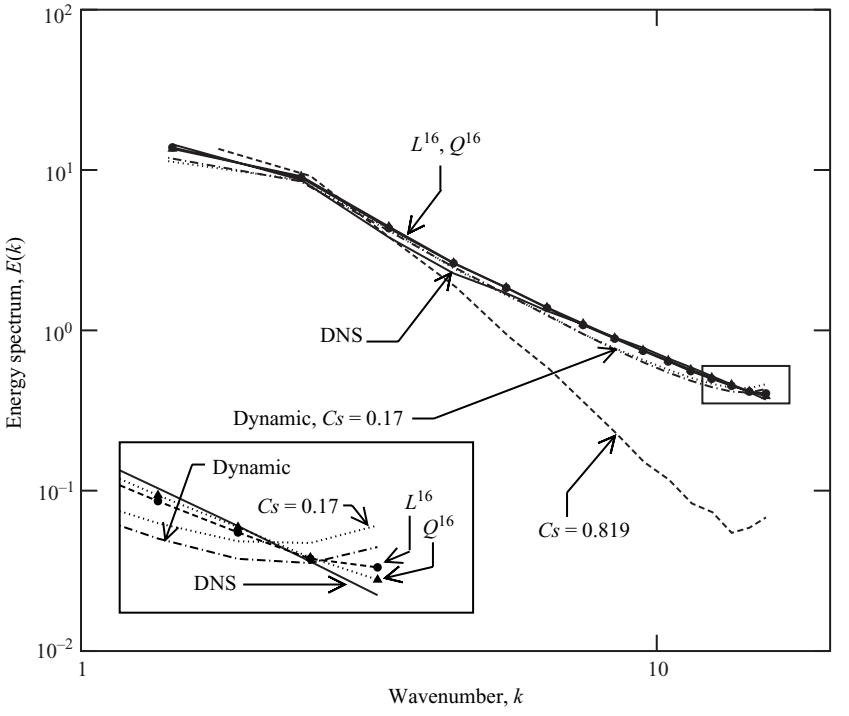


FIGURE 2. The three-dimensional energy spectrum, $E(k)$, for filtered DNS and $32^3$ LES with an optimal linear model ($L^{16}$), an optimal quadratic model ($Q^{16}$), two cases of a Smagorinsky model ($Cs = 0.17$ and $Cs = 0.819$) and the dynamic Smagorinsky model (Dynamic).

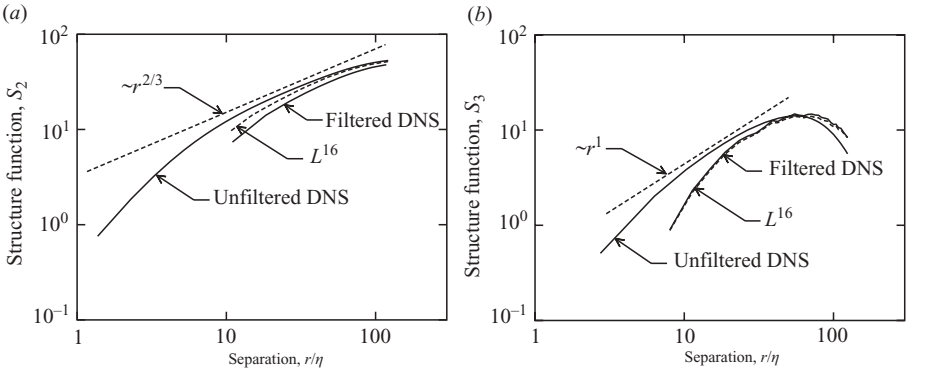


FIGURE 3. (*a*) Second-order structure function $S_2 = \langle |\Delta \boldsymbol{u}|^2 \rangle$ and (*b*) third-order structure function $S_3 = \langle |\Delta \boldsymbol{u}|^3 \rangle$ for the DNS velocity $\boldsymbol{u}$, the filtered DNS velocity $\tilde{\boldsymbol{u}}$, and the LES velocity $\boldsymbol{w}$ from an optimal linear LES ($L^{16}$).

the subgrid (the dissipation) when measured in an *a priori* test, again indicating the difference between *a posteriori* and *a priori* performance, though in this case that difference in performance is actually quite small.

The energy spectrum $E(k)$ is a second-order statistical quantity, which can also be represented in physical space as a second-order structure function. The structure function $S_2(r) = \langle |\boldsymbol{w}(\xi + \boldsymbol{r}) - \boldsymbol{w}(\xi)|^2 \rangle$ is shown in figure 3(*a*) for the optimal linear model

($L^{16}$) and the filtered and unfiltered DNS. There is relatively good agreement between the LES data and the filtered DNS data. The slight shift between the two curves arises due to a discrepancy between the mean filtered kinetic energy of the two systems. This is equal to the error in $E(k)$ (see figure 2) integrated over $k$, so it is apparent that the mid-spectrum discrepancies in $E(k)$ lead to the shift in $S_2(r)$. Overall, the linear model does a good job of predicting the correct second-order structure function.

In isotropic turbulence, two-point third-order statistics can be represented through the third-order structure function $S_3(r) = \langle |\boldsymbol{w}(\xi + \boldsymbol{r}) - \boldsymbol{w}(\xi)|^3 \rangle$, which is shown in figure 3(*b*) for the optimal linear model ($L^{16}$), and the DNS. The agreement between the LES data and the filtered DNS data is nearly perfect. We might argue that the second-order statistics $E(k)$ and $S_2(r)$ were likely to be correct, because second-order DNS statistics were built into the subgrid model. This argument fails because the use of second-order statistics in the model only guarantees an *a priori* match in statistics; it does not guarantee that an actual simulation will generate the correct results. However, not even an *a priori* claim can be made about the third-order statistics for the optimal linear model. This provides further support that the optimal linear model embodies many of the important characteristics of the ideal model. In particular, the third-order structure function is important in the transfer of energy between different wavenumbers.

Finally, note that the second- and third-order structure functions for the unfiltered DNS data are also shown in figure 3. It is clear that these quantities are not equal to the structure functions computed for the filtered DNS data. We may be tempted to make an argument that 'small scales are lost' in filtering and so the filtered structure functions should be affected only for the small separations. However, figure 3 shows that this would be a mistake. Also, the differences in structure function shown are specific to the sharp Fourier-cutoff filter. In general, details of the LES filter must be known before we can sensibly compare LES results to real turbulence. More importantly, when LES is used as a predictive tool, we are not interested in the statistics of the filtered fields, but rather the statistics of the real turbulence. Thus, in addition to the usual LES subgrid stress models discussed here, models are required for the subgrid contribution to whatever statistical quantities are of interest. While important, this issue is not addressed here.

## 3. Effects of filter shape

The impact of filter shape on the performance of LES models is investigated here by considering three different graded filters: a Gaussian filter, a top-hat filter and an exponential filter. As in § 2, the analysis and simulations here are performed using Fourier spectral representations. Thus, filtering and de-filtering operations are performed in wave space by multiplying or dividing (respectively) by the Fourier transformed filter kernel. Further, the graded filters are combined with a cutoff filter ($k_c = 16$), as explained in § 1.1. Finally, note that the grading of the filter directly impacts the model kernels, because they are determined from filtered statistical correlations, as shown in (1.6) to (1.8).

### 3.1. *Definitions of filter shapes*

All the graded filters considered here are isotropic, and are defined by a filter kernel $g$ such that

$$\boldsymbol{w}(\boldsymbol{x}) = \int g(\boldsymbol{x} - \boldsymbol{x}')\boldsymbol{u}(\boldsymbol{x}')\,\mathrm{d}\boldsymbol{x}'. \tag{3.1}$$

Let $G(\boldsymbol{k})$ denote the Fourier transform of $g(\boldsymbol{x})$. Since the filters are isotropic, $G$ and $g$ are both functions of a single scalar argument. Considered are three classes of filters, a top-hat filter, a Gaussian filter and an exponential filter. Both the top-hat and Gaussian are commonly used in LES, the exponential filter is also considered here to allow a more general class of filter shapes. The spherically symmetric top-hat filter is defined as

$$g(\xi) = \begin{cases} 6/(\pi\Delta^3), & \xi < \Delta/2, \\ 0, & \text{otherwise}, \end{cases} \qquad G(k) = \frac{12(2\sin(k\Delta/2) - k\Delta\cos(k\Delta/2))}{k^3\Delta^3}. \tag{3.2}$$

The Gaussian filter is defined as

$$g(\xi) = \frac{(6/\pi)^{3/2}}{\Delta^3}\exp(-6\xi^2/\Delta^2), \qquad G(k) = \exp(-k^2\Delta^2/24). \tag{3.3}$$

The exponential filter is defined as

$$G(k) = \exp(-k\ln(\gamma)/k_c), \tag{3.4}$$

where $\gamma$ corresponds to the amplification at the filter cutoff. This filter is similar to the Gaussian, except that the dependence of the exponent on $k$ is linear instead of quadratic. Note that when $\gamma > 1$, the exponential filter actually amplifies the small scales.

In the Gaussian and top-hat filters, $\Delta$ is a characteristic filter width, and the filters have all been normalized to be mean-preserving ($G(0) = 1$), in three dimensions.

Since the above filters will be combined with a Fourier-cutoff as the projection, it is convenient to describe the filter parameter $\Delta$ in terms of the Fourier-cutoff parameter $k_c$. Let $h = \pi/k_c$, which is the Nyquist grid spacing for the the cutoff wavenumber $k_c$. Then, for the top-hat and Gaussian filters, the cases considered are $\Delta = h$, $2h$ and $3h$. For the exponential filter, the cases considered are $\gamma = 0.1$, 0.5, 0.9, 1.1 and 2.0; this filter is already parameterized in terms of $k_c$. Filter kernels are shown in figure 4. Note that in the case of $\Delta = 3h$, $G(k)$ for the top-hat filter is slightly negative for $k > 0.96k_c$.

### 3.2. *Effect of filter shape on subgrid force magnitude*

One of the more obvious effects of varying the filter shape is that the subgrid force changes, particularly the magnitude of the subgrid force. This is important because a larger subgrid force means that the LES model is responsible for more of the dynamics of the filtered field. To compare subgrid force magnitude (measured *a priori*) with different filters meaningfully, it is normalized by the magnitude of the exact filtered time derivative. Let $\hat{\boldsymbol{M}}^{/\dot{\boldsymbol{u}}}$ denote the normalized squared spectral magnitude of the subgrid force:

$$\hat{\boldsymbol{M}}^{/\dot{\boldsymbol{u}}} = \frac{\langle \hat{M}_i(\boldsymbol{k})\hat{M}_i^*(\boldsymbol{k})\rangle}{\left\langle \widehat{\frac{\partial \hat{u}_i(\boldsymbol{k})}{\partial t}}\,\widehat{\frac{\partial \hat{u}_i^*(\boldsymbol{k})}{\partial t}} \right\rangle}. \tag{3.5}$$

The relative subgrid force magnitude $\hat{\boldsymbol{M}}^{/\dot{\boldsymbol{u}}}$ was computed for each filter, and is shown in figure 5. It is immediately clear that the sharp Fourier-cutoff filter produces

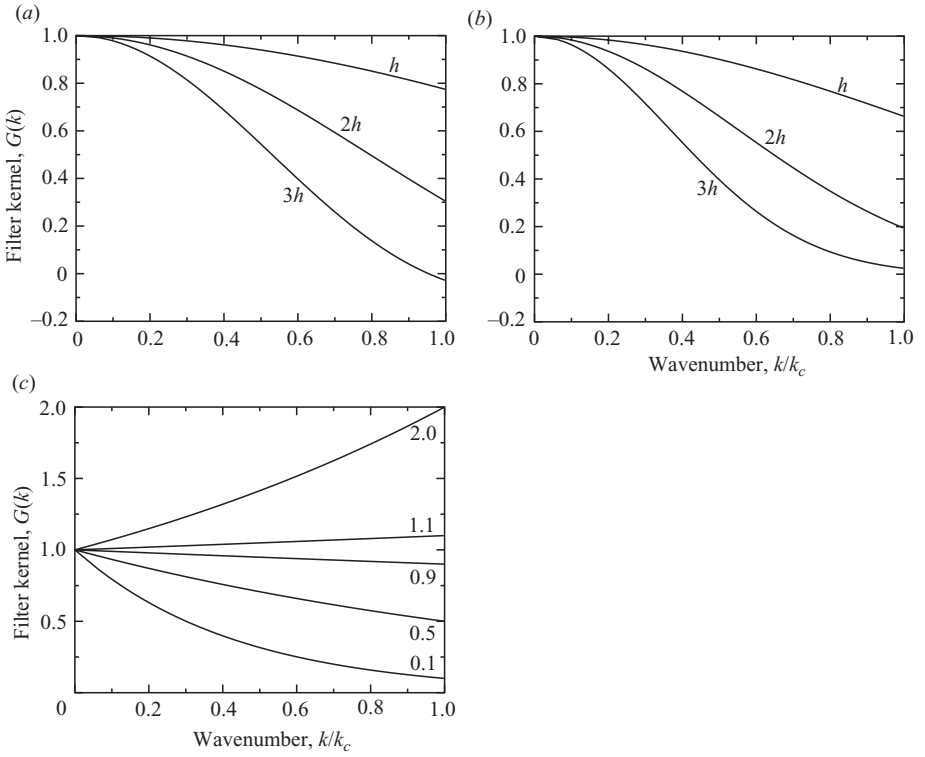


FIGURE 4. Filter kernels for (*a*) top-hat filters, (*b*) Gaussian filters and (*c*) exponential filter. In (*a*) and (*b*), $\Delta = h$, $2h$ and $3h$, where $h = \pi/k_c$ is the grid spacing. In (*c*), $\gamma = 0.1$, 0.5, 0.9, 1.1 and 2.0. The value of $\gamma$ corresponds to the amplification at the filter cutoff.

a smaller subgrid force than any other filter shown here, except for the exponential filter with $\gamma = 1.1$, which has only a marginally smaller subgrid force.

To understand this observation, begin with the Navier–Stokes equations in Fourier space:

$$\frac{\partial}{\partial t}\hat{u}_i(\boldsymbol{k}) = -\nu k^2 \hat{u}_i(\boldsymbol{k}) - \mathscr{P}_{ijk}(\boldsymbol{k}) \int_{\boldsymbol{k}'} \hat{u}_j(\boldsymbol{k}')\hat{u}_k(\boldsymbol{k}-\boldsymbol{k}')\,\mathrm{d}\boldsymbol{k}', \tag{3.6}$$

where

$$\mathscr{P}_{ijk} = \mathrm{i}k_k\left(\delta_{ij} - \frac{k_i k_j}{k^2}\right). \tag{3.7}$$

In large-eddy simulation, we write a similar equation for the filtered field, which is then

$$\begin{aligned}\frac{\partial}{\partial t}(G(k)\hat{u}_i(\boldsymbol{k})) &= -\nu k^2 (G(k)\hat{u}_i(\boldsymbol{k})) \\ -\mathscr{P}_{ijk}(\boldsymbol{k}) &\int_{\boldsymbol{k}'} (G(k')\hat{u}_j(\boldsymbol{k}'))(G(k-k')\hat{u}_k(\boldsymbol{k}-\boldsymbol{k}'))\,\mathrm{d}\boldsymbol{k}' \\ -\mathscr{P}_{ijk}(\boldsymbol{k}) &\int_{\boldsymbol{k}'} (G(k) - G(k')G(k-k'))\hat{u}_j(\boldsymbol{k}')\hat{u}_k(\boldsymbol{k}-\boldsymbol{k}')\,\mathrm{d}\boldsymbol{k}'.\end{aligned} \tag{3.8}$$

The first and second terms in this equation have been written so that the original

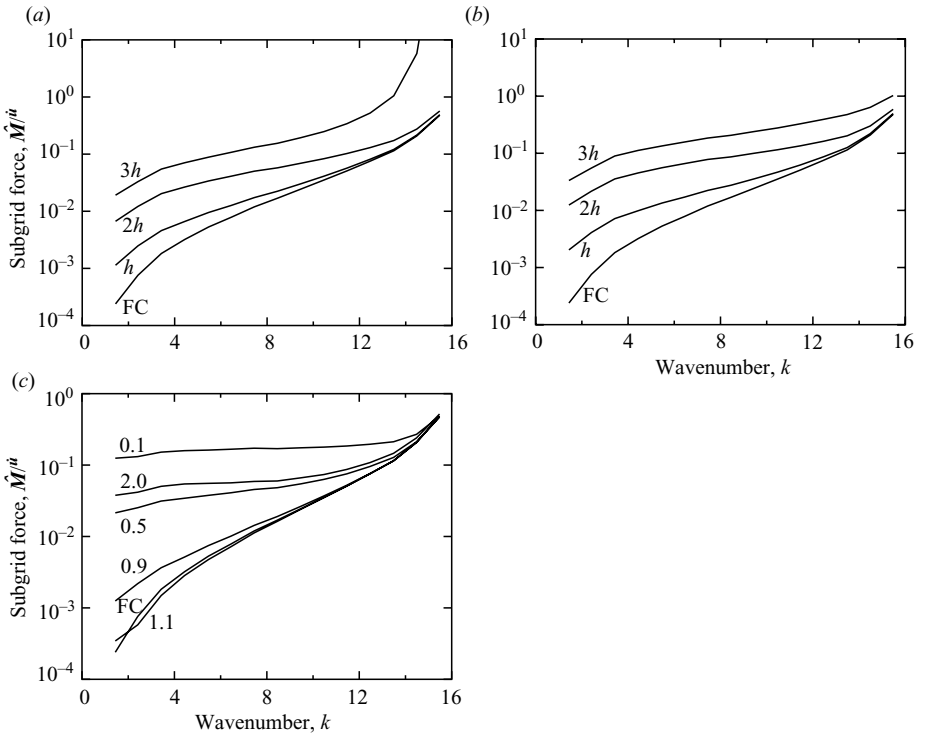


FIGURE 5. Relative subgrid force, $\hat{M}^{/\hat{u}}$, for the (*a*) top-hat filter, (*b*) Gaussian filter and (*c*) exponential filter. Also shown is the sharp Fourier cutoff filter (FC). In (*a*) and (*b*), $\Delta = h$, $2h$ and $3h$. In (*c*), $\gamma = 0.1$, 0.5, 0.9, 1.1 and 2.0.

structure of the governing equations is preserved; however, the state variable is now $\hat{\tilde{\boldsymbol{u}}} = G(k)\hat{\boldsymbol{u}}(\boldsymbol{k})$ instead of $\hat{\boldsymbol{u}}(\boldsymbol{k})$. The third term in this equation is the subgrid force, so that

$$\hat{M}^{/\hat{u}} = \frac{\left\langle \left| \mathscr{P}_{\alpha jk}(\boldsymbol{k}) \int_{\boldsymbol{k}'} (G(k) - G(k')G(k-k'))\hat{u}_j(\boldsymbol{k}')\hat{u}_k(\boldsymbol{k}-\boldsymbol{k}')\,\mathrm{d}\boldsymbol{k}' \right|^2 \right\rangle}{\left\langle \left| \dfrac{\partial \widetilde{\hat{u}_\alpha(\boldsymbol{k})}}{\partial t} \right|^2 \right\rangle} \tag{3.9}$$

is the normalized subgrid force magnitude being measured.

It is clear that the subgrid force can be trivially made zero if $G(k) = 1$ for all $k$. However, in this case, the filter would do nothing, and any simulation would essentially be a DNS. The filters considered here are all non-invertible, with the property that $G(k) = 0$ for $k > k_c$. Still, setting $G(k) = 1$ for $k < k_c$ ensures that the integrand in (3.9) vanishes for part of the integration region. This suggests, but does not prove, that the sharp Fourier-cutoff filter should have a smaller relative subgrid force than the other filters. It is possible to do better than the sharp cutoff filter, though not with a Gaussian or top-hat filter. It was seen that $\hat{M}^{/\hat{u}}$ was slightly smaller for the exponential filter with $\gamma = 1.1$ than for the sharp Fourier-cutoff filter. This raises the question of what filter shape would minimize $\hat{M}^{/\hat{u}}$. Such an optimization could be done if we had a full set of quartic statistics (four-point quartic correlations), but such data are not currently available.

### 3.3. *Effect of filter shape on estimation differences*

It was shown above that the subgrid force is almost always smallest when a sharp Fourier-cutoff filter is used. This alone suggests that errors will most probably be smallest for the cutoff filter, since the term to be modelled is smaller. However, it is possible for a larger model term to in some way be easier to model. To evaluate this possibility, the *a priori* estimation differences have also been determined for each filter shape. In Langford & Moser (1999), the estimation differences were normalized by the magnitude of the term being estimated (i.e. the subgrid force), which was an excellent measure of how much of the subgrid force can be captured by the model. However, this normalization does not allow for a valid comparison of the effects of different filters because subgrid force magnitude is filter dependent, as seen in § 3.2

A better normalization for the current purposes is

$$\hat{\boldsymbol{E}}^{/\bar{\boldsymbol{u}}} = \frac{\langle \hat{d}_i(\boldsymbol{k}) \hat{d}_i^*(\boldsymbol{k}) \rangle}{\left\langle \widetilde{\frac{\partial \hat{u}_i(\boldsymbol{k})}{\partial t}} \widetilde{\frac{\partial \hat{u}_i^*(\boldsymbol{k})}{\partial t}} \right\rangle}, \tag{3.10}$$

which shows the expected impact of the estimation difference on the dynamics of the filtered system. Here, $d_i = M_i - m_i$ is the estimation difference. More importantly, this measure gives an unbiased indication of the dependence of the difference on the filter shape. To see this, consider de-filtering the numerator and denominator of (3.10), by dividing them by $G^2(k)$ for $k \leqslant k_c$. The value of the ratio is unchanged, but the denominator is then the projected (i.e. Fourier-cutoff filtered) exact time derivative, and the numerator can be interpreted as the difference measured in the Fourier-cutoff filtered equations of the following computational procedure for the nonlinear and subgrid force terms: (i) apply the invertible shaped filter to the projected velocities, (ii) compute the nonlinear term and subgrid force model based on the filtered projected velocity, (iii) de-filter (using the invertible filter) the nonlinear terms and model term to use in the projected equations. Thus, $\hat{\boldsymbol{E}}^{/\bar{\boldsymbol{u}}}$ is an estimation difference measure in a consistent set of equations (the Fourier-cutoff filtered equations), which indicates the impact of a graded filter, on the computation of the nonlinear term and subgrid model.

$\hat{\boldsymbol{E}}^{/\bar{\boldsymbol{u}}}$ is plotted for the three filter families considered here in figure 6, for linear estimation models. It is evident that the Gaussian and top-hat filters offer a small improvement over the cutoff filter for wavenumbers very close to the cutoff, but at a cost of significantly increased error throughout the remainder of the spectrum. However, it is near the cutoff that the modelling errors have the largest impact on the dynamics, so this improvement may be of value in an LES. It is also evident that the reduced magnitude of the subgrid force for the exponential filter with $\gamma = 1.1$ did not yield a significant improvement in the estimation errors.

### 3.4. *Effect of filter shape on a posteriori error*

The results of §§ 3.2–3.3 suggest that there is little motivation for the use of graded filters in addition to a Fourier-cutoff filter. The errors are in most cases larger than in the Fourier-cutoff case and the burden carried by the model is actually increased when the Gaussian and top-hat filters are used. However, the Gaussian and top-hat filters with $\Delta = 2h$ have somewhat smaller errors near $k_c$, and the exponential filter with $\gamma = 1.1$ produces a slightly smaller model term. Whether these properties are important in a simulation can only be determined by performing the simulations.

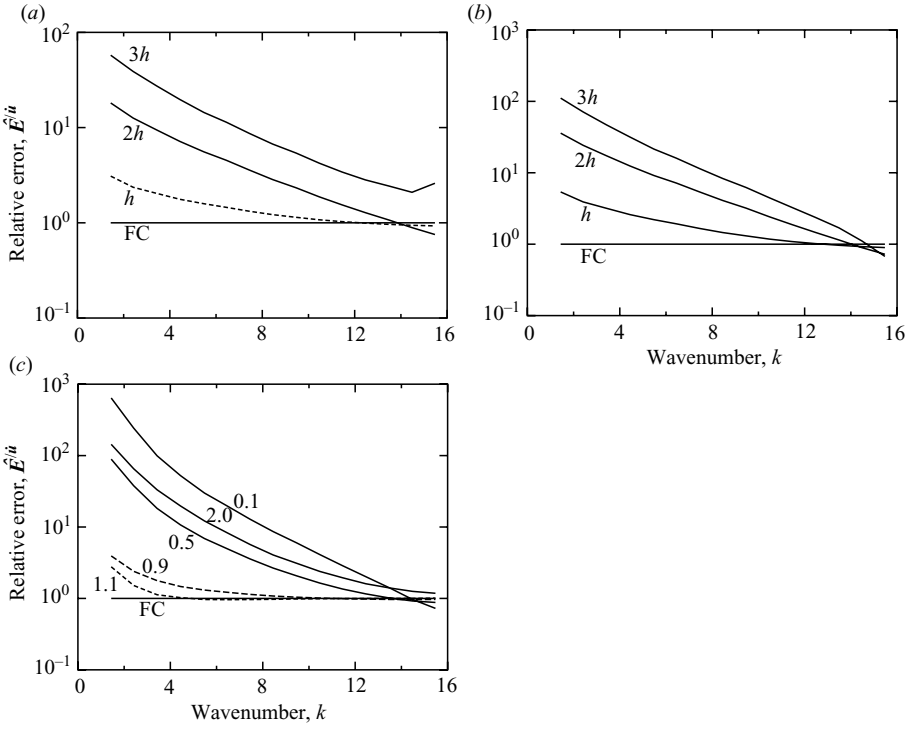


FIGURE 6. Relative linear estimation difference, $\hat{E}^{/\bar{u}}$, for the (*a*) top-hat filters, (*b*) Gaussian filters and (*c*) exponential filters. In (*a*) and (*b*), $\Delta = h, 2h, 3h$; in (*c*), $\gamma = 0.1, 0.5, 0.9, 1.1, 2.0$. Differences are normalized such that the difference for the sharp Fourier-cutoff filter (FC) is 1.

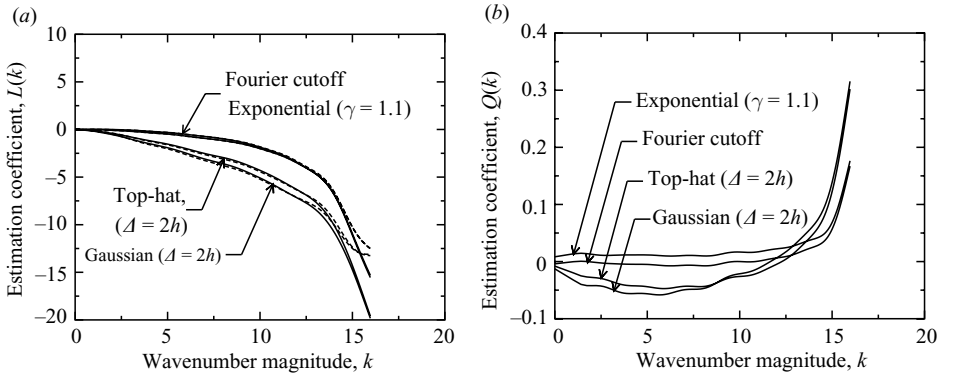


FIGURE 7. Estimation coefficients, (*a*) $L(k)$ for a linear model (solid) and a quadratic model (dashed), and (*b*) $Q(k)$ for various filters.

Both linear and quadratic models were used in simulations using each of the three filter shapes ($\Delta = 2h$ and $\gamma = 1.1$). The model functions $L(k)$ and $Q(k)$ are shown in figure 7. Results for simulations using the quadratic model (linear model results are similar) are shown in figure 8. The spectra from the simulations with graded filters have been 'de-filtered' to allow direct comparison with the DNS and Fourier cutoff spectra. Note that the spectra from the top-hat and Gaussian filter simulations are in poor

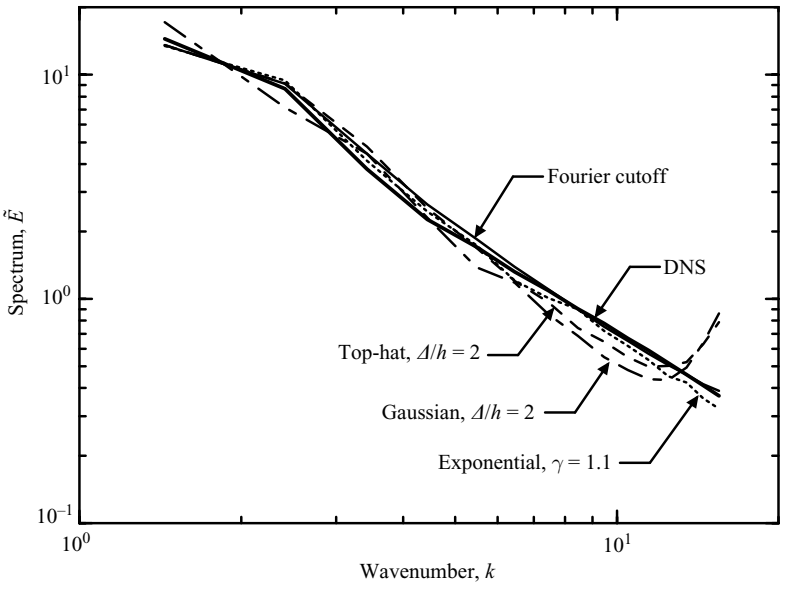


FIGURE 8. Spectra from LES with quadratic optimal models and several different filters compared to that from DNS. $\tilde{E}(k) = E(k)/G^2(k)$ is the de-filtered spectrum.

agreement with the DNS near the filter cutoff. The $\gamma = 1.1$ exponential filter produces a better spectrum, but it is slightly inferior to that from the Fourier cutoff simulation.

The results of this section indicate that the use of graded filters in addition to a Fourier cutoff filter increases the difficulty of modelling the subgrid force. The magnitude of the model term is generally increased, as is the *a priori* and *a posteriori* error. Of course, we could use a graded filter, and invert the graded component of the filter before computing the nonlinear terms, and apply the graded filter to the results. This procedure would recover the Fourier cutoff filter results. In this case, the use of the graded filter is not harmful, but it is pointless.

As mentioned in § 1.3, other authors have identified a number of reasons to avoid Fourier cutoff filters in LES, so the question naturally arises as to why it appears so attractive here. With regard to the lack of guaranteed positivity of the subgrid stress, the resulting realizability constraints on the model are not used in the optimal procedure, so this causes no difficulties. Further, it should be noted that none of the filters considered here (cutoff filters with grading) yield guaranteed positive stresses. Realizability constraints are generally useful in formulating other models, but this may still be possible with cutoff filters because it is the conditional average of $\tau_{ij}$ ($\langle \tau_{ij} | \boldsymbol{w} \rangle$) that we need to model, and it may still be generally positive with cutoff filters. Other difficulties associated with cutoff filters arise from Gibbs phenomena (Meneveau & Katz 2000; Leslie & Quarini 1979), which results in strongly wavenumber-dependent eddy viscosity and a large convective component of the subgrid term (Eyink 1994), though this is presumably largely stochastic. While these features may be annoying in some contexts, they do not affect how well the deterministic subgrid effects can be modelled, which is what is being assessed here.

One possible reason the Fourier cutoff filter may be particularly good in LES is that the Fourier coefficients associated with different wavenumbers are uncorrelated. As a consequence, all quadratic forms, particularly energy and dissipation, are partitioned between the large and subgrid scales. This and the orthogonality of the Fourier modes,

limits the ways in which the large scales and subgrid scales defined through a Fourier-cutoff filter can interact through a quadratic nonlinearity, both instantaneously and on average. Also, we observed that the cutoff filter yielded smaller-magnitude subgrid terms, which presumably leaves less to be modelled. The orthogonality of the Fourier modes makes the Navier–Stokes terms in (1.2) equivalent to the Galerkin projection of the Navier–Stokes equations into the LES space, which has the property of minimizing the residual in the projected equation (the subgrid term), which is consistent with our observations. None of the properties of Fourier cutoff filtering mentioned here conclusively determines that such filters will be particularly good for LES, but they do suggest that the good performance of the cutoff filter in the tests used here are not fortuitous.

## 4. Effects of model non-locality

Recall that our estimates have been expressed as convolutions of the velocity field with an estimation kernel $L(r)$. The most obvious way to introduce a locality restriction is to simply require that $L(r)=0$ for $r>r_{max}$, so that only velocity data at a distance of up to $r_{max}$ is included in the estimate. However, for functions for which the Taylor series has an infinite radius of convergence, such as the cutoff filtered velocity, information from distances further than $r_{max}$ manifests itself in the derivatives at $r=0$, so the field at a distance can be reconstructed using the local information. Thus, a local estimate obtained by restricting the region of integration is no different from a global estimate.

A better way to investigate locality is to consider estimates of the subgrid force that depend only on velocity at a discrete set of nearby points. To do this, we can express $L(r)$ as a linear combination of delta functions:

$$L(r)=\sum_{i=1}^{N}\alpha_i\delta(r-r_i). \tag{4.1}$$

Delta functions have a sifting property, so a convolution of (4.1) with the velocity field is equivalent to a linear combination of discrete velocity values. We have written the estimation kernel $L(r)$ as a single function of distance, $r$, to preserve the spherical symmetry of the estimation kernel. Thus, the estimation of subgrid force is actually a linear combination of discrete shell-averaged velocity values, which does not correspond to what we would encounter in a practical LES using finite-volume, finite-difference or finite-element methods. This rather artificial situation arises because the spectral representations used here are not a natural context in which to explore issues of spatial localization of estimates. Several insights can none-the-less be gained in this idealized setting.

The analogue of (4.1) in Fourier space is

$$\hat{L}(k)=\sum_{i=0}^{N}\alpha_i\frac{\sin(kr_i)}{kr_i}. \tag{4.2}$$

Optimal kernels were computed for two cases: $r_i=ih$, with $N=r_{max}/h$ so that $r_i\leqslant r_{max}$; and $r_i=ih/N$, so that $r_i\leqslant h$. The resulting kernels in wave space ($\hat{L}(k)$) are shown in figures 9–10, for several values of $N$ and $r_{max}$. In figure 9($a$), it is clear that as $r_{max}$ increases, $\hat{L}(k)$ becomes closer to the optimal global model. In figure 10, the case with four values of $r_i$ ($N=3$) produces an optimal $\hat{L}(k)$ which is almost the same as the global model. Yet the model is spatially local, showing that a restriction on

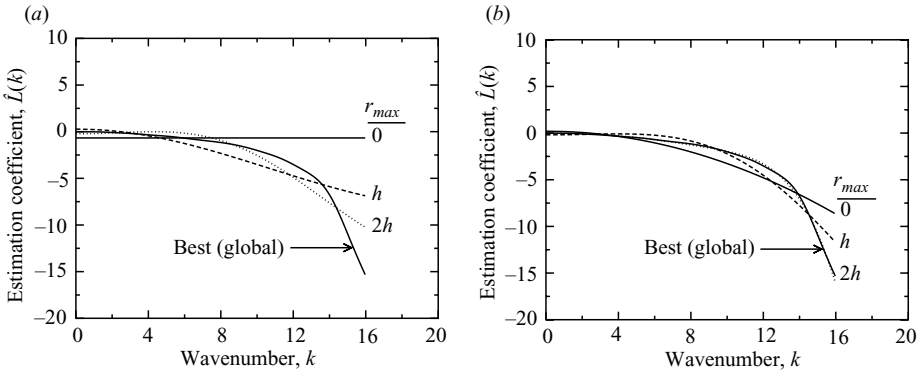


FIGURE 9. Optimal estimation coefficient $\hat{L}(k)$ for a localized expansion consisting of impulses spaced evenly at 0, $h$, $2h$, ..., $r_{max}$, for various values of $r_{max}$. Event data consists of ($a$) LES velocities; ($b$) LES velocities and the second derivative evaluated at $r = 0$.

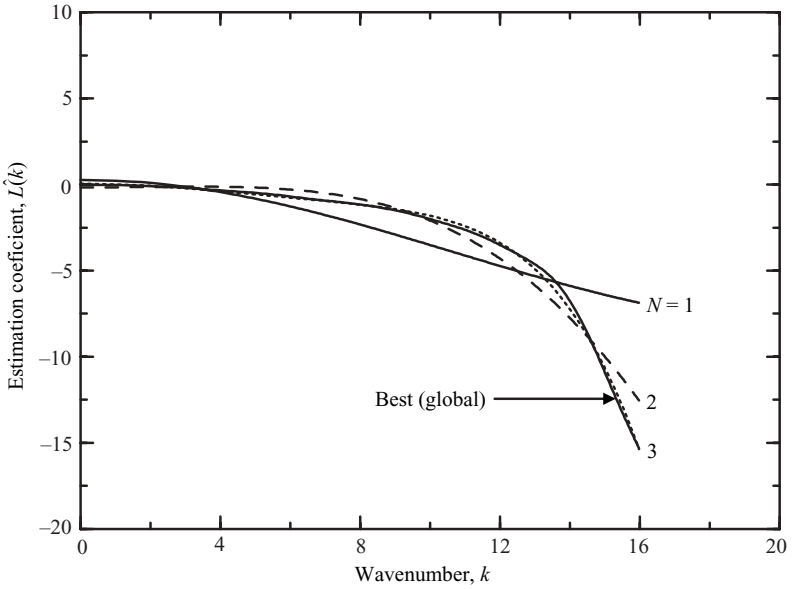


FIGURE 10. Optimal estimation coefficient $\hat{L}(k)$ for a localized expansion consisting of $(N+1)$ impulses evenly spaced between 0 and $h$, for various values of $N$.

spatial locality does not inherently limit the capability of the model. Clearly, in this case, by making the $r_i$ more closely spaced, we are approaching the situation discussed above in which the field in the region $r < r_{max}$ provides the same information as the entire field. Four points with $r_i \leqslant h$ were sufficient to reproduce the global model, suggesting that a completely local model (perhaps at just one point) in which a small number of derivatives are included in the event data would suffice to produce a good approximation to the global model.

The most natural way to measure the effects of spatial locality in the current context is to restrict the spacing of the $r_i$ to $h$, as would be the case in an LES using non-spectral methods, and to restrict the number of derivatives considered in the event data, also consistent with practice in practical LES. Derivative event

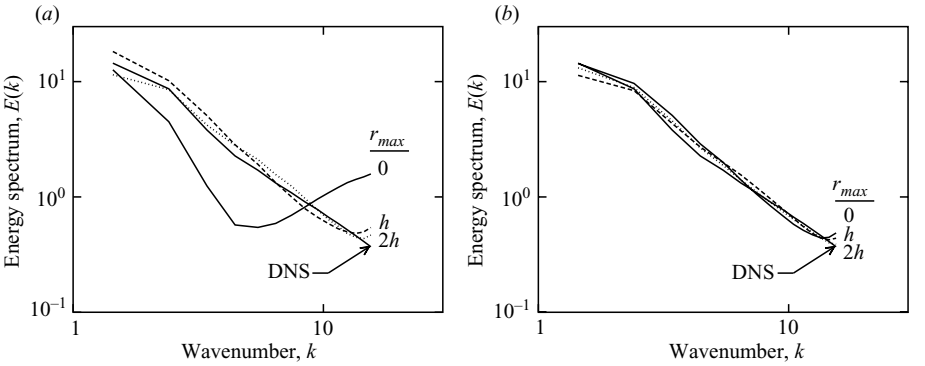


FIGURE 11. Three-dimensional energy spectrum, $E(k)$, for LES conducted with optimal estimation coefficient $\hat{L}(k)$ from a localized expansion consisting of impulses spaced evenly at $0, h, 2h, \ldots, r_{max}$, for various values of $r_{max}$. Event data consist of ($a$) LES velocities, ($b$) LES velocities and the second derivative evaluated only at $r = 0$.

data at $r = 0$ is useful because it can replace non-local information through Taylor series expansion. The effectiveness of low-order derivatives in providing non-local information is evaluated by including the second derivative of velocity as an event in the estimation. The models that result when such a procedure is applied, with and without the second derivative are shown in figure 9($b$). It seems that the estimation kernel $\hat{L}(k)$ for $r_{max} = 2h$ provides a good approximation to the global model.

To evaluate the importance of the variations of the local models from the global model, simulations were conducted for the $\hat{L}(k)$ shown in figure 9. *A posteriori* results for the three-dimensional energy spectrum, $E(k)$, are shown in figure 11. For each case, the high-wavenumber portion of $E(k)$ hooks up incorrectly, and the significance of the discrepancy decreases as non-local event data is added. However, the simulation results are actually quite good, and the $r_{max} = 2h$ case with second derivative events is nearly as good as the global linear estimate shown in figure 2. As locality is restricted, the estimation kernels $\hat{L}(k)$ change considerably (see figure 9), whereas the simulation results do not, except for the $r_{max} = 0$ case in figure 11($a$), which clearly does not include enough information in the event data.

## 5. Discussion and conclusions

Through a series of *a priori* and *a posteriori* tests in isotropic turbulence, the performances of optimal LES models have been evaluated in several situations: with Fourier cutoff filters, with so-called graded filters and with both global and local dependence of the models. These tests serve to both characterize the performance of the optimal models and to explore the impact of filter grading and model localization. The following specific conclusions can be drawn from the results reported here:

($a$) The optimal LES models proposed by Langford & Moser (1999) for isotropic turbulence with Fourier cutoff filters do indeed produce highly accurate large-eddy simulations, despite the measured r.m.s. difference between the models and the actual subgrid force being large (approximately 90% of the subgid term) when measured *a priori*. This is consistent with many previous observations that LES models often produce accurate simulations while performing poorly in *a priori* tests. These results lend further weight to the conjecture of Langford & Moser (1999) that the large difference between the model and subgrid force in these models is due to a similarly

large discrepancy between the ideal (minimum difference) model and the real subgrid term; that is, that the subgrid force is primarily stochastic. Note that this does not imply that performance on such *a priori* tests is irrelevant, only that the target for the difference between the model and the actual term is not zero, but the minimum possible, which is attained by the ideal model and which may in fact be large.

(*b*) The use of graded filters in conjunction with a Fourier cutoff projection does not appear to be advantageous in LES. The graded filters studied here yield larger subgrid force terms, so that the model must account for a larger fraction of the dynamics. Further, when linear and quadratic optimal LES models are used, the *a priori* estimation errors are larger than with the cutoff filter, and the Fourier cutoff filter produces the most accurate *a posteriori* spectrum. Since the optimal models used here are quite general, and are optimized for the specific filter being used, these results suggest that the graded filters will, in general, degrade the modelability of the subgrid term.

Of course, we can construct models that perform well for graded filters by inverting the grading (if invertible). Such de-filtering models have been pursued by several authors (e.g. Domaradzki & Loh 1999; Stolz *et al.* 2001); see the review by Domaradzki & Adams (2002). However, de-filtering by itself cannot replace the information eliminated by the non-invertible projection, so further modelling is still required. Current results suggest that the filter grading does not help make this modelling easier.

A significant shortcoming of Fourier cutoff filters is that they are difficult or impossible to implement in general complex geometries, and for this reason other filters are often more appropriate. The current results simply suggest that when performing an LES with Fourier spectral methods, adding a graded filter to the implicit Fourier truncation is probably not helpful.

(*c*) Optimal LES models are naturally formulated to allow the subgrid force at any point to depend on the LES field in the entire flow domain. However, this is apparently not necessary. In the cases studied here, a model that is dependent only on the LES velocities at discrete distances spaced by one filter width, up to a maximum distance of just three filter widths is enough to reproduce nearly the global optimal model results. Further, when dependency on second derivatives is included in the model dependence, non-locality can be further reduced to two or even one filter width, depending on the acceptable level of error.

It is interesting to observe the role that optimal LES modelling plays in drawing the above conclusions. Once the good performance of the optimal models is confirmed (as above), the optimal models can be used as a surrogate for a wide range of possible subgrid models. Because the optimal models are optimized for each specific filter and locality restriction, the results represent the best that is possible using models with forms subsumed by the optimal model and formulated *a priori*. By using these general models rather than a more conventional model (e.g. Smagorinsky), we were able to obtain results on the impact of filtering and locality on model performance that are applicable more generally than for one specific model. Thus, the above conclusions on the inadvisability of graded filters in addition to a Fourier cutoff, and the locality of model dependence are likely to be applicable to LES in general.

### 5.1. *Toward practical optimal LES*

In this paper, we have demonstrated the performance of optimal models constructed using DNS statistical correlations, and used these models to explore the impact of filter shape and model locality. Using DNS data in this way allows us to explore the

properties of the models without introducing uncertainties that would be associated with modelling the statistical input to the optimal models. However, if optimal LES models are to be useful in actual LES, they must be formulated without appeal to DNS statistical data. Fortunately, this appears to be possible. For quadratic estimation models such as those considered here, the small-separation second-, third- and fourth-order multi-point correlations are needed. Provided the separations are in a Kolmogorov inertial range and small-scale isotropy can be assumed, the Kolmogorov scaling theory and the quasi-normal approximation are sufficient to specify most of the required statistical information. The rest can be obtained using a dynamic procedure similar to that used in the dynamic model (Germano *et al.* 1991).

Another prerequisite for optimal models to be useful is that they be formulated using more generally applicable large-scale representations than the Fourier spectral representation. The most promising is a finite-volume representation, in which the state variables are the velocities averaged over discrete volumes. In essence, the filter is a discretely sampled top-hat. This allows the LES to be formulated in quite general geometries. Finite-volume optimal LES is currently being developed (Zandonade *et al.* 2004), and it is being formulated using theoretical statistical information.

Also of concern in practical LES is the computational cost of evaluating the model terms. In general, this depends on the details of the optimal formulation and its implementation. For the quadratic models used here and those being used in finite-volume optimal LES, the cost of evaluating the models is negligible because the models are of the same form as the terms in the Navier–Stokes equations.

This research was jointly supported by the National Science Foundation and the Air Force Office of Scientific Research under NSF grant CTS-9616219, NSF grant CTS-001435 and AFOSR grant F49620-01-1-0181 and by NASA grant NGT 2-52229. We would also like to thank R. Adrian and S. Balachandar for their insightful comments. We are especially grateful to Mr Paulo Zandonade for performing some of the Smagorinsky model simulations.

## REFERENCES

Adrian, R. 1977 On the role of conditional averages in turbulence theory. In *Turbulence in Liquids* (ed. J. Zakin & G. Patterson), pp. 323–332. Science Press, Princeton, New Jersey.

Adrian, R. 1990 Stochastic estimation of sub-grid scale motions. *Appl. Mech. Rev.* **43**, 214–218.

Adrian, R., Jones, B., Chung, M., Hassan, Y., Nithianandan, C. & Tung, A. 1989 Approximation of turbulent conditional averages by stochastic estimation. *Phys. Fluids* **1**, 992–998.

Bardina, J., Ferziger, J. & Reynolds, W. 1980 Improved subgrid-scale models for large-eddy simulation. *AIAA Paper* 80-1357.

Boris, J., Grinstein, F., Oran, E. & Kolbe, R. 1992 New insights into large eddy simulation. *Fluid Dyn. Res.* **10**, 199–228.

Carati, D., Winckelmans, G. S. & Jeanmart, H. 2001 On the modelling of the subgrid-scale and filtered-scale stress tensors in large-eddy simulation. *J. Fluid Mech.* **441**, 119–138.

Clark, R., Ferziger, J. & Reynolds, W. 1979 Evaluation of subgrid-scale models using an accurately simulated turbulent flow. *J. Fluid Mech.* **91**, 1–16.

Domaradzki, J. A. & Adams, N. A. 2002 Direct modelling of subgrid scales of turbulence in large eddy simulaitons. *J. Turbulence* **3** (024).

Domaradzki, J., Metcalfe, R., Rogallo, R. & Riley, J. 1987 Analysis of subgrid-scale eddy viscosity with use of results from direct numerical simulations. *Phys. Rev. Lett.* **68**, 547–550.

Domaradzki, J. A. & Loh, K.-C. 1999 The subgrid-scale estimation model for high Reynolds number turbulence. *Phys. Fluids* **11**, 2330–2342.

Eyink, G. L. 1994 Energy-dissipation without viscosity in ideal hydrodynamics 1: Fourier-analysis and local energy-transfer. *Physica* D **78**, 222–240.

Germano, M., Piomelli, U., Moin, P. & Cabot, W. 1991 A dynamic subgrid-scale eddy viscosity model. *Phys. Fluids* **3**, 1760–1765.

Ghosal, S., Lund, T., Moin, P. & Akselvoll, K. 1995 A dynamic localization model for large-eddy simulation of turbulent flows. *J. Fluid Mech.* **286**, 229–255.

Kraichnan, R. 1976 Eddy viscosity in two and three dimensions. *J. Atmos. Sci.* **33**, 1521–1536.

Langford, J. & Moser, R. 1999 Optimal LES formulations for isotropic turbulence. *J. Fluid Mech.* **398**, 321–346.

Lesieur, M. & Métais, O. 1996 New trends in large-eddy simulations of turbulence. *Annu. Rev. Fluid Mech.* **28**, 45–82.

Lesieur, M. & Rogallo, R. 1989 Large-eddy simulation of passive scalar diffusion in isotropic turbulence. *Phys. Fluids* **1**, 718–722.

Leslie, D. & Quarini, G. 1979 The application of turbulence theory to the formulation of subgrid modelling procedures. *J. Fluid Mech.* **91**, 65–91.

Lilly, D. 1992 A proposed modification of the Germano subgrid-scale closure method. *Phys. Fluids* **4**, 633–635.

Liu, S., Meneveau, C. & Katz, J. 1994 On the properties of similarity subgrid-scale models as deduced from measurements in a turbulent jet. *J. Fluid Mech.* **275**, 83–119.

Meneveau, C. & Katz, J. 2000 Scale-invariance and turbulence models for large-eddy simulation. *Annu. Rev. Fluid Mech.* **32**, 1–32.

Meneveau, C., Lund, T. & Cabot, W. 1996 A Lagrangian dynamic subgrid-scale model of turbulence. *J. Fluid Mech.* **319**, 353–385.

Métais, O. & Lesieur, M. 1992 Spectral large-eddy simulation of isotropic and stably stratified turbulence. *J. Fluid Mech.* **239**, 157.

Pope, S. B. 2000 *Turbulent Flows*. Cambridge University Press.

Rogallo, R. & Moin, P. 1984 Numerical simulation of turbulent flows. *Annu. Rev. Fluid Mech.* **16**, 99–137.

Smagorinsky, J. 1963 General circulation experiments with the primitive equations. *Mon. Weather Rev.* **91**, 99–164.

Stolz, S., Adams, N. A. & Kleiser, L. 2001 An approximate deconvolution model for large-eddy simulation with application to incompressible wall-bounded flows. *Phys. Fluids* **13**, 997–1015.

Vreman, B., Geurts, B. & Kuerten, H. 1994 Realizability conditions for the turbulent stress tensor in large-eddy simulation. *J. Fluid Mech.* **278**, 351–362.

Winckelmans, G. S., Wray, A. A., Vasilyev, O. V. & Jeanmart, H. 2001 Explicit-filtering large-eddy simulation using the tensor-diffusivity model supplemented by a dynamic Smagorinsky term. *Phys. Fluids* **13**, 1385–1403.

Zandonade, P. S., Langford, J. A. & Moser, R. D. 2004 Finite-volume optimal large-eddy simulation of isotropic turbulence. *Phys. Fluids* **16**, 2255–2271.

Zhou, Y., Hossain, M. & Vahala, G. 1989 A critical look at the use of filters in large eddy simulations. *Phys. Lett.* A **139**, 330.